Review of Air-Sea Transfer Processes

James B. Edson

University of Connecticut, Avery Point, Department of Marine Sciences
Groton, USA
james.edson@uconn.edu

1. Background

Investigations of atmospheric turbulence over the world's oceans have shown that the interaction of wind with surface waves results in flow characteristics that differ substantially from even a horizontally homogeneous terrestrial surface layer. A simple illustration of this is given by consideration of the surface roughness. Over land, the surface roughness can often be treated as constant or slowly varying due to vegetative changes. Over the ocean, the surface roughness or drag is determined by the wave field, which is largely determined by the wind – the stronger the winds, the rougher the seas. Therefore, the exchange of momentum and energy is largely governed by the wave field near the ocean surface.

Above this, lies a layer where the turbulent flow is governed by the generation of turbulence by wind shear and its generation/suppression by buoyancy/stratification. Many turbulent statistics obey Monin-Obukhov similarity (Obukhov 1946; Monin and Obukhov 1954) in this region, which states that these turbulent statistics are universal function of z/L after normalization by the appropriate scaling parameters. Here, z is the height above the surface and L is known as the Monin-Obukhov (MO) length, which represents the height at which the generation of turbulence by shear and buoyancy are equal.

As a result, marine meteorologists and physical oceanographers often divide the boundary layer close to the ocean surface into the surface layer where wind shear and buoyancy/stratification govern the turbulent flow (i.e., an MO layer) and a wave boundary layer (WBL) where additional scaling parameters are required for similarity. Even though the search for these scaling parameters and hypotheses for their use has been going on for many years (e.g., Charnock, 1955; Donelan et al., 1993; Hare et. al, 1997; Johnson et al., 1998), we are still a long way from a consensus in the scientific community.

This overview presents results from several field programs that we specifically designed to investigate the interaction of turbulent flow over surface waves in the marine surface layer. These investigations rely on a set of data collected from the R/P FLIP and an offshore tower during the Marine Boundary Layer (MBL, Hristov et al., 2003), Risø Air-Sea Experiment (RASEX, Mahrt et al., 1996) and Coupled Boundary Layer and Air-Sea Transfer (CBLAST, Edson et al., 2007) programs sponsored by the Office of Naval Research. In addition, the overview takes advantage of a data set collected during the NSF sponsored CLIvar MOde Water Dynamic Experiment (CLIMODE) conducted during two winter seasons in the North Atlantic about the northern wall of the Gulf Stream. The Gulf Stream region of the North Atlantic is a very attractive region for air-sea interaction research as the region experiences the largest net wintertime heat loss over the global ocean with climatological estimates approaching 400 W/m^2. Frequent wintertime storms drive near surface winds and momentum flux that often exceed 15 m/s and 1.0 N/m^2, respectively.

2. Exchange Coefficients

The exchange of momentum and energy between the atmosphere and ocean is difficult to measure directly over the ocean. Instead, oceanographers and meteorologist often rely on bulk formula that relates the fluxes to more easily measured averaged wind speed, temperature and humidity. These averaged variables are

related to the flux through transfer coefficients. For example, based on the dimensional arguments, the exchange of momentum at the ocean surface is expected to go as the wind speed squared:

$$\tau = -\rho_a \overline{uw} = \rho_a C_D U_r^2 \tag{1}$$

where τ is the momentum flux or surface stress, ρ_a is the density of air, $\overline{uw}$ represents the momentum flux where the overbar denotes a time average; U_r is the wind speed relative to water (i.e., the air-water velocity difference) and C_D is the transfer coefficient for momentum known as the drag coefficient. These transfer coefficients are typically parameterized as a function of atmospheric stability and surface roughness as

$$C_D(z/z_o, z/L) = \frac{-\overline{uw}}{U_r^2} = \left(\frac{\kappa}{\ln(z/z_o) - \psi_u(z/L)} \right)^2 \tag{2}$$

$$C_H(z/z_{oT}, C_D^{1/2}, z/L) = \frac{-\overline{wT}}{U_r \Delta\Theta} = C_D^{1/2} \left(\frac{\kappa}{\ln(z/z_{oT}) - \psi_T(z/L)} \right) \tag{3}$$

$$C_E(z/z_{oq}, C_D^{1/2}, z/L) = \frac{-\overline{wq}}{U_r \Delta Q} = C_D^{1/2} \left(\frac{\kappa}{\ln(z/z_{oq}) - \psi_q(z/L)} \right) \tag{4}$$

where C_T and C_q are transfer coefficient for temperature and humidity known as the Stanton and Dalton numbers, $\overline{wT}$ and $\overline{wq}$ represents the heat and moisture fluxes; z is the height above the surface; $\Delta\Theta$ and ΔQ are the mean air-sea temperature and specific humidity differences; L is the MO length, κ is the von Karman constant, z_o is the aerodynamic roughness lengths; z_{oT} and z_{oq} are the roughness lengths for temperature and humidity, respectively; and ψ_m, ψ_H and ψ_M are the functions that account for the effects of atmospheric stratification for momentum, heat and mass exchange, respectively.

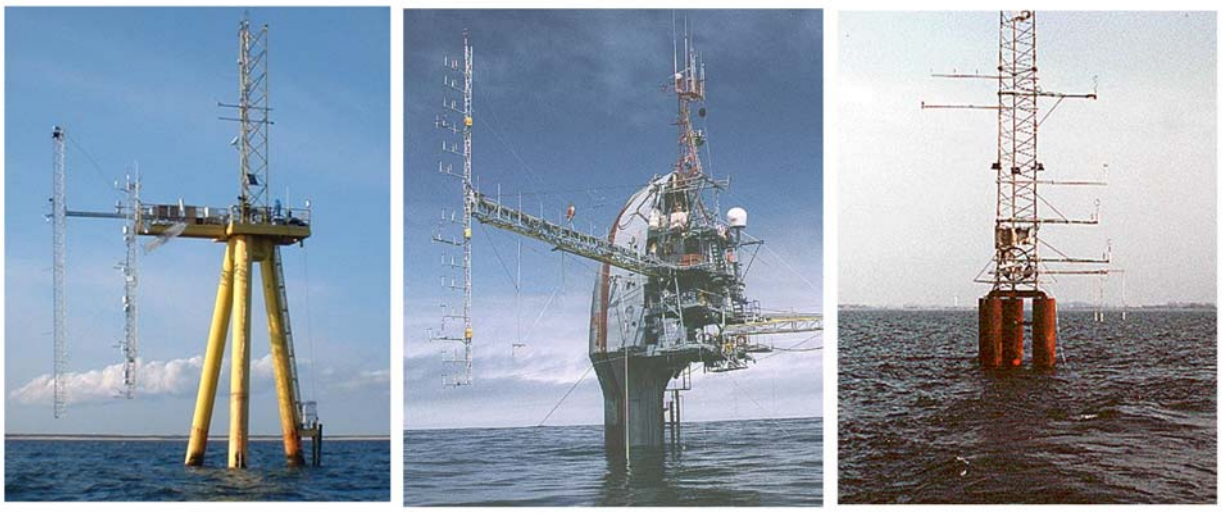

Figure 1. Three platforms used to directly measure flux-profile relationships during the CBLAST and MBL/RASEX programs. The ASIT tower used in CBLAST is at left, the R/P FLIP used in MBL is shown in the center, and the tower used in the RASEX program is shown at right.

2.1. Dimensionless Shear

To improve our parameterizations of C_D and the other transfer coefficients for later use, we have to directly measure the momentum, heat and mass fluxes along with the mean relative wind speed, temperature and humidity. For example, the $\psi_x(z/L)$ functions represent a stability correction that is related to the integral of the dimensionless gradients $\phi_x(z/L)$

$$\varphi_x(z/L) = \frac{\kappa z}{x_*}\left[\frac{\partial X}{\partial z}\right] \tag{5}$$

where

$$\psi_x(z/L) = \int [1-\phi_x(z/L)]\frac{d(z/L)}{z/L} \tag{6}$$

and u_* is the velocity scaling parameter known as the friction velocity and $x_* = (-\overline{wx}/u_*)$ is the scaling velocity for the variable $x = u, T, q$. Determination of these stability functions or flux-profile relationships therefore require fluxes and their associated gradients. Flux-profile measurements were made during the ONR sponsored MBL/RASEX (Vickers and Mahrt, 1999) and CBLAST programs (Edson et al., 2006), which utilized the two oversea towers as shown in Figure 1.

Measurements of the dimensionless shear from the CBLAST and RASEX experiments are shown in Figure 2. The bin-average data agree very well with the current formulations used in the COARE 3.0 algorithm, which is based on over land and over ice experiments. The data provides a von Karman constant of 0.4, which is the most commonly assigned value in the literature. Although there are some small systematic

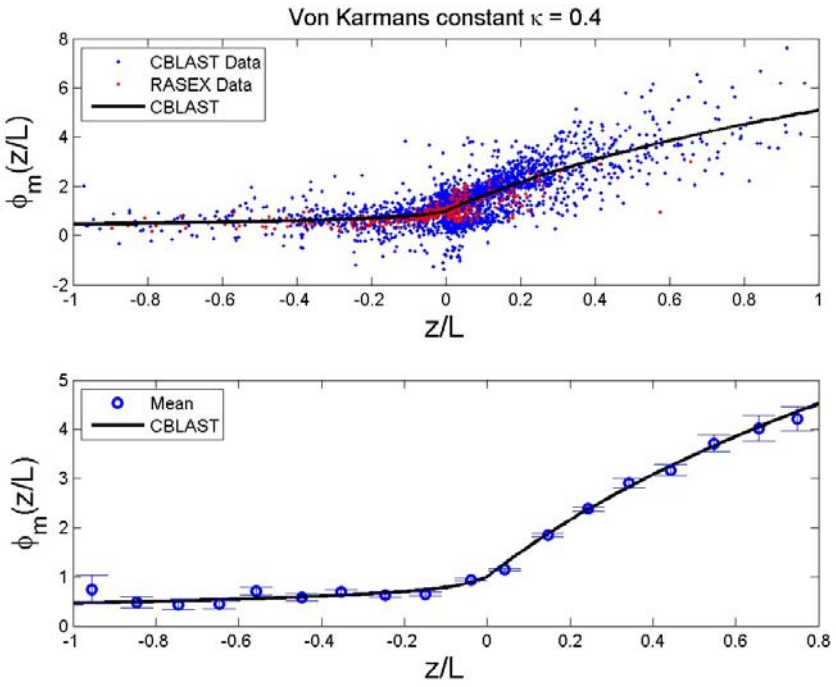

Figure 2. Estimates of the dimensionless shear versus the stability parameter z/L from the CBLAST and RASEX programs. The black line represents a slight modification to the COARE 3.0 algorithm to account for lower values of the dimensionless shear under unstable conditions (z/L <0). The top panel shows the individual data from each experiment and the bottom panel is averaged over stability bins.

differences between the COARE 3.0 algorithm under certain wave conditions, the agreement is remarkable. Similar agreement is found for the dimensionless scalar profiles under unstable conditions. There is substantially more uncertainty in the scalar functions under stable conditions, but the same can be said for over land surface layers. Therefore, the use of flux-profile relationships based on MO similarity is valid in the marine surface layer.

3. Momentum Exchange

The inclusion of the measurements made during the CLIMODE experiment allows an investigation of the transfer coefficients at high wind speeds. The momentum, heat and mass fluxes were provided by three highly instrumented platforms during the field program to provide surface fluxes using the direct covariance technique: a moored 3-m discus buoy, a research vessel for surveys, and a drifting Air-Sea Interaction Spar (ASIS). The ship and ASIS packages included Direct Covariance Flux Systems (DCFS) used in the development of the COARE bulk algorithm. The DCFS's deploy on the research vessel and ASIS included a sonic anemometer, infrared hygrometer and motion correction system that provide estimates of the momentum, sensible heat and latent heat fluxes using the direct covariance method. A low powered version of the DCFS was deployed for 15 months on a 3-m discus mooring. A low-power version of the DCFS was deployed on the discus mooring and operated successfully for over a year. Fluxes from the ASIS and discus buoy (Figure 3) have been combined with data taken from stabilized platforms and fixed towers in previous field studies to validate and improve the bulk formula. The combined data set a wide range of wind speed, sea state, and atmospheric stability conditions to improve the bulk flux formula.

Figure 3. Two of the platforms used during the CLIMODDE program to provide direct covariance estimates of the momentum and heat fluxes. The 3-m discus mooring that was successfully deployed for 15 months in the Gulf Stream is shown at left, while the Air-Sea Interaction Spar (ASIS) is shown at right.

3.1. Wind-Speed Dependent Formulation

The drag coefficient is commonly parameterized in terms of a roughness length. In the COARE 3.0 algorithm (Fairall et al., 2003), the roughness length, z_0, is parameterized using a wind speed dependent formulation, i.e., the stronger the wind, the rougher the surface and the greater the drag:

$$z_0 = \alpha(U_r)\frac{u_*^2}{g} \tag{7}$$

where α is a wind-speed dependent parameter known as the Charnock coefficient and g is the gravitational acceleration. The Charnock coefficient can be thought of as an inverse Froude number as it represents the ratio of the gravitational restoring force to the inertial forces (i.e., the wind stress) generating the roughness elements. As such, this parameterization represents the roughness of the gravity-capillary waves, which support the majority of the surface stress at wind speeds greater than approximately 4 m/s. As the wind speed and surface stress increases, so does the roughness length given by **(7)**.

Direct estimates of the stability corrected (neutral) drag coefficient are shown in Figure 4 along with the COARE 3.0 algorithm. The neutral drag coefficients are in good agreement with COARE 3.0 over moderate wind conditions. However, there are differences at the lowest and highest wind speeds where COARE 3.0 overestimates and underestimates the drag, respectively. Fairly simple modifications to the COARE 3.0, which is designated as COARE 4.0, provide excellent agreement with the merged data set.

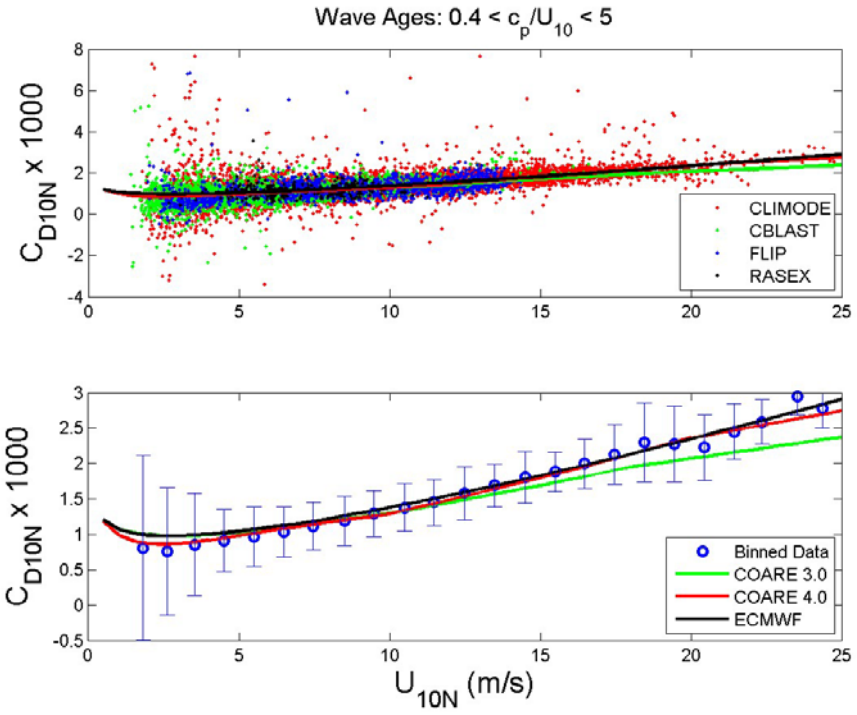

Figure 4. Direct estimate of the drag coefficient plotted versus wind speed. The values have been corrected for atmospheric stability using MO similarity theory (Fairall et al., 2003). The range of wave ages used in the plot is given and no ship data is included in the analysis to reduce the effect of flow distortion. The top panel shows the individual data from each platform and the bottom panel is averaged over wind-speed bins. The green line represents the COARE 3.0 algorithm, while the red line is a modification to the COARE 3.0 algorithm designated as COARE 4.0. The black line is the function provided by ECMWF, which is based on a wave-age dependent formulation for the stress. These stress estimates were globally averaged as a function of wind speed to determine the wind-speed dependent function shown.

3.2. Wave-Age Dependent Formulation

Another common approach to modeling the drag coefficient is to parameterize the surface roughness as a function of wave-age, c_p/U_{10}, where c_p is the phase speed of the dominant wave. The combined data set covers a wide range of wave-ages as shown by Figure 5. Briefly, fully-developed (mature) seas have a wave age of approximately one, i.e., the wave speed and wind speed are approximately equal. Values less than one

indicate developing (young) seas, while values greater than one indicate decaying (old) seas. This approach is attractive because the waves represent physically the roughness elements that support the exchange of momentum across the air-sea interface once the sea is fully rough. Measurements show that the ocean is typically rougher the younger the wave field at a given wind speed. Therefore, one might expect a wave-age dependent drag coefficient to provide a better estimate of the surface drag than a wind speed dependent formulation at any given wind speed. In fact, researchers commonly attribute some of the scatter in Figure 4 to processes that cannot be represented by the wind speed alone such as the duration of a wind event, the fetch over which the wind is blowing, the depth of the water, etc – all of which affect the wave-age.

Unfortunately, it is not always easy to compare drag coefficients based on wind speed with those based on wave-age because of the potential mismatch between atmospheric forcing and the state of the underlying sea. Fortunately, the European Centre for Medium-range Weather Forecasts (ECMWF) has determined a wind speed dependent drag coefficient based on the drag computed in their coupled model (Hersbach, Chelton, & Janssen, personal communication). The ECMWF parameterization is based on a wave-age dependent surface roughness that relies on ECMWF's wave model. The drag coefficient therefore represents globally averaged wave-age dependent roughness at a given wind speed.

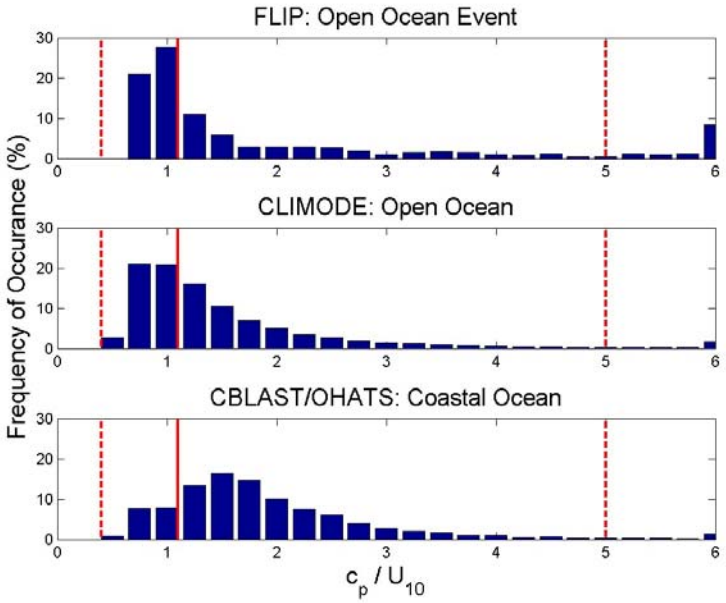

Figure 5. The frequency of occurrence of wave-ages from 3 different field programs. The solid red line is the wave-age commonly associated with fully-developed seas. The broken line defines the range of wave-ages used to generate Figure 4.

The function representing the globally averaged drag coefficient is plotted versus wind speed in Figure 4. The agreement between the measurements and the ECMWF parameterization is remarkable given the range of conditions encountered in the two data sets. Perhaps more surprising is the agreement between ECMWF and the COARE 4.0 algorithm given the nature of the two parameterizations. Specifically, ECMWF (and many wave modelers) parameterizes the surface roughness as a function of the inverse wave-age defined as u_* / c_p:

$$z_0 = \alpha(u_* / c_p)\frac{u_*^2}{g} \qquad \textbf{(8)}$$

where α is now the Charnock coefficient as a function of inverse wave-age.

3.3. Reconciling Wind-Speed and Wave-Age Dependent Formulations

An explanation for the excellent agreement between the two formulations of the surface roughness (and thereby the drag coefficient) can be found by looking at the relationship between inverse wave-age and wind speed shown in Figure 6. Research has shown that a fully developed sea occurs at $u_* / c_p \approx 0.03$, which is indicated by the broken line in Figure 6. However, the measurements indicate that fully developed seas are rarely found and that the relationship is quite linear over a wide range of wind-speeds. These results indicate that the strong winds found under mid-latitudes storms simply do not remain over the same group of waves long enough to become fully developed due to the different propagation speeds of the storm and wave field. As such, young waves are always found under high wind conditions, and old waves (generated from non-local winds) are found under low wind conditions. Therefore, the linear relationship between inverse wave-age and wind speed can be used to convert the wave-age dependent roughness length to a wind speed dependent roughness length:

$$\alpha(u_* / c_p) \quad \Rightarrow \quad u_* / c_p = f(U_r) \quad \Rightarrow \quad \alpha(u_* / c_p) \approx \alpha(U_r) \tag{9}$$

The resulting wind-speed dependent roughness length closely matches the proposed COARE 4.0 parameterization.

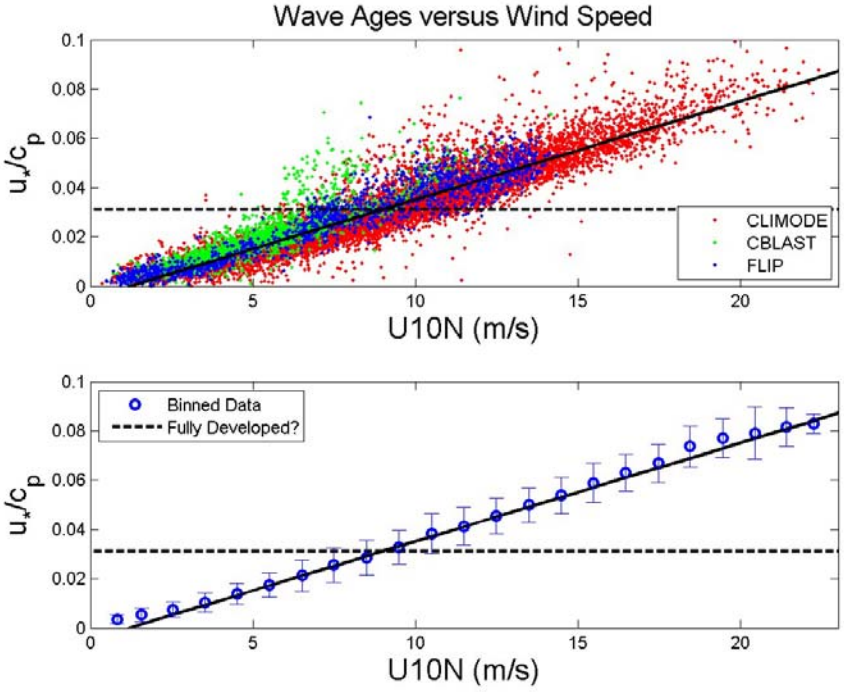

Figure 6. Inverse wave-age plotted versus wind speed. The top panel shows the individual data from each experiment and the bottom panel is averaged over wind-speed bins. The broken black line represents the inverse wave-age commonly associated with fully-developed seas The solid line provides a linear relationship between inverse wave-age and wind speed given by $u_* / c_p = 0.004 U_{10N} - 0.005$.

3.4. Low Wind Speeds

At lower wind speeds, the surface roughness often parameterized in terms of the roughness Reynolds number (i.e., the ratio of the inertial to viscous forces), which results in:

$$z_0 = \beta \frac{\nu}{u_*} \tag{10}$$

where ν is the kinematic viscosity and β is a constant determined to be 0.11 from laboratory experiments. This parameterization causes the roughness length to increase as the wind speed decreases and viscous forces dominate the exchange of momentum. The COARE 3.0 algorithm follows the approach described by Smith (1980) where the two roughness parameterizations are added together to find the total roughness. As such, the roughness length and thereby the drag coefficient is expected to have a minimum at winds speeds around 3 m/s.

There is clear evidence for this minimum in Figure 4. However, the bin-average drag coefficients fall below the COARE parameterization at the lowest wind speed. This discrepancy is more significant in the CBLAST data set (Edson et al., 2007), which was almost always swell-dominated at low wind speeds. Therefore, it has been hypothesized that wind-swell interaction is the leading cause for the reduction of the drag a low winds. This has been supported by the Large Eddy Simulations (LES) of wind-swell interaction reported by Sullivan *et al*. (2008). The LES results indicate that the dominant forces above the waves in this region are a wave-induced momentum flux divergence that accelerates the flow and a retarding pressure gradient, i.e., opposite to the momentum balance in classical boundary layers. Under these conditions, the wave driven winds produce a low-level jet and a rapid decay of the momentum flux with height. This upward exchange of momentum is expected to reduce the total momentum flux, which would act to reduce the drag under these conditions.

4. Heat Exchange

The transfer coefficient for the buoyancy flux is shown in Figure 7. The buoyancy flux is defined as

$$\overline{wT_v} = \overline{wT} + 0.61T\,\overline{wq} = -C_B U_r \Delta\Theta_v \qquad \textbf{(11)}$$

where the negative sign is required because $\Delta\Theta_v$ is defined as the virtual potential temperature difference between the air and sea. This flux is very closely related to the heat flux computed by a sonic anemometer, and contains contributions from both the latent and sensible heat fluxes. Estimates of the buoyancy transfer coefficient are in reasonably good agreement with the COARE 3.0 algorithm for wind speeds less than 15 m/s. However, there are significant differences with C3.0 at higher winds. Therefore, the data is now being used to reduce the uncertainty in the transfer coefficients for wind speeds greater than 15 m/s. Of particular interest are the extreme conditions encountered during cold air outbreaks that drive combined latent and sensible heat fluxes exceed 1200 W/m^2. These enormous heat fluxes are driven by high winds and large air-sea temperature and humidity differences.

Under these conditions, a number of studies have shown that evaporating sea-spray begins to have a noticeable impact on the heat exchange. For example, the reduction of the buoyancy transfer coefficient could be related to the effects of sea spray. However, the contribution of both latent and sensible heat to this flux makes it difficult to determine the impact of sea-spray. In fact, the original version of the TOGA-COARE algorithm known as COARE 2.6 is in better agreement with these results at high winds. Therefore, it is necessary to separate the fluxes into the latent and sensible heat flux, so we can investigate their respective transfer coefficients directly.

For example, the CBLAST measurements indicate that the COARE 3.0 bulk aerodynamic formulation represents direct-covariance measurements of latent heat flux accurately when the latent heat flux is positive (corresponding to an upward moisture flux), but poorly when the latent heat flux is negative (corresponding to a downward moisture flux). The downward latent heat flux is often associated with fog and stable conditions (Edson et al., 2004). However, the CBLAST data indicates that the Dalton numbers (i.e., the transfer coefficient for latent heat) remain lower than the COARE algorithm parameterization even after

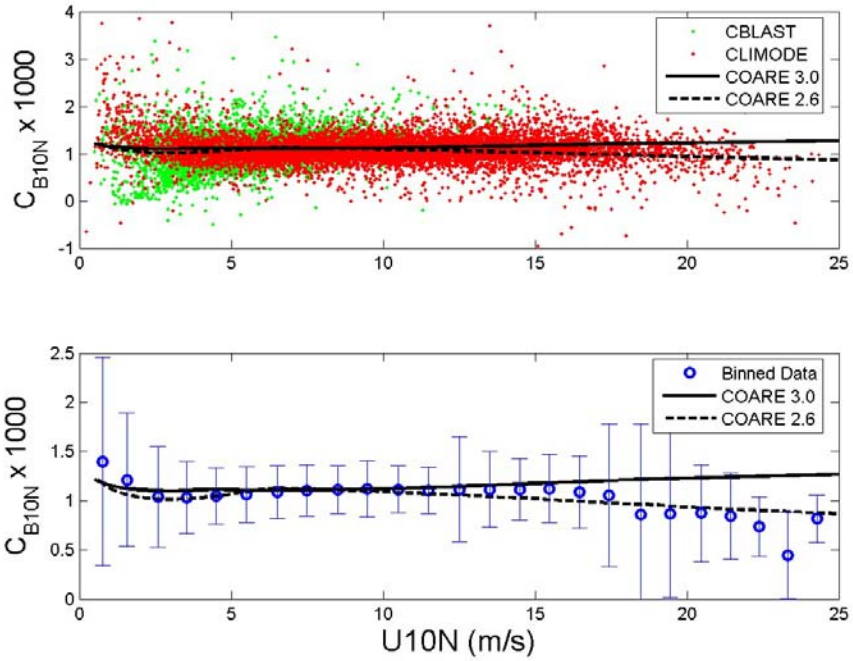

Figure 7. Direct estimates of the transfer coefficient for the buoyancy flux taken from the CBLAST and CLIMODE programs. The solid black line shows the COARE 3.0 parameterization, while the broken line shows the original COARE 2.6 parameterization. The top panel shows the individual data from each experiment and the bottom panel is averaged over wind-speed bins.

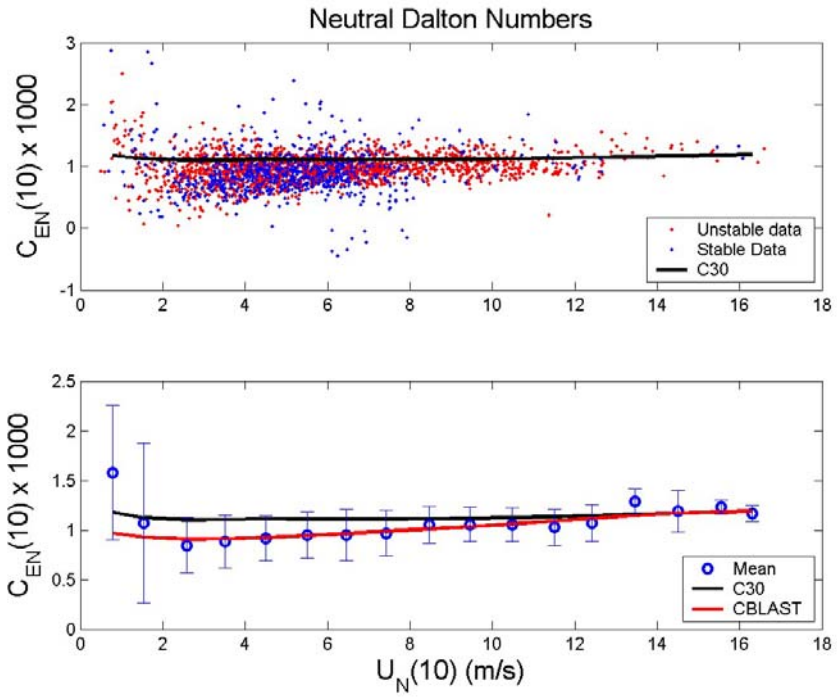

Figure 8. Individual and bin-averaged estimates of the neutral Dalton number. The black lines represents the COARE 3.0 parameterization, while the red line represents the proposed CBLAST parameterization.

removal of downward fluxes and foggy periods as shown in Figure 8. Therefore, the CBLAST algorithm proposes a neutral Dalton number that is 25% lower than the COARE algorithm at low winds speed. On the other hand, the Stanton numbers (i.e., the transfer coefficient for sensible heat) is in reasonable agreement with COARE 3.0 as shown in Figure 9. This result argues against the commonly held assumption that the neutral transfer coefficients for heat and mass are equal. Separate latent and sensible heat flux estimates from the CLIMODE experiment are being combined with the CBLAST data to investigate these processes – including spray.

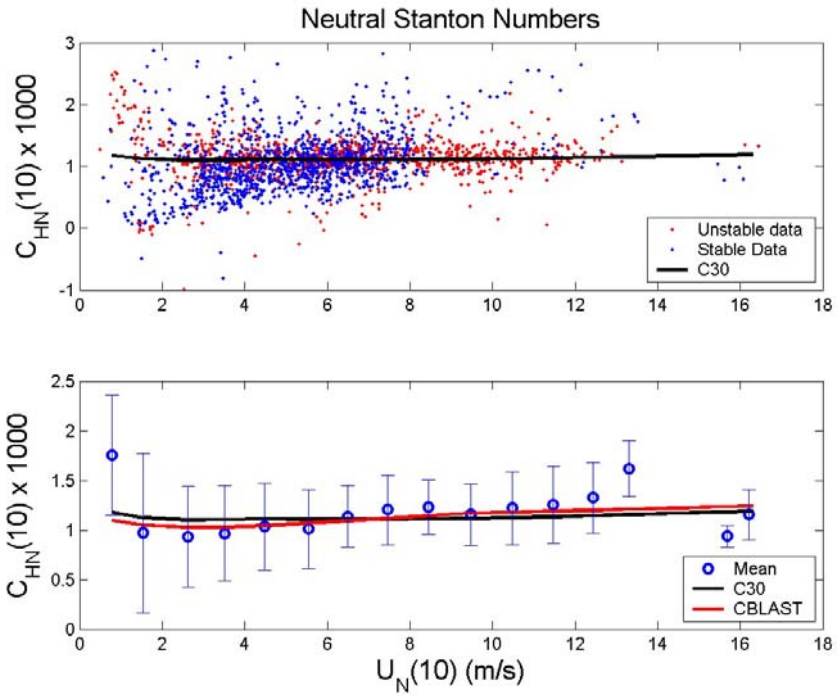

Figure9. Individual and bin-averaged estimates of the neutral Stanton number. The black lines represents the COARE 3.0 parameterization from Fairall et al. (2003), while the red line represents the proposed CBLAST parameterization.

5. Energy Exchange

The significant amount of kinetic energy (KE) transported from the atmosphere to the ocean represents a fundamental difference between the ocean and terrestrial boundary layers. To demonstrate this, we begin with an expression for the KE flux at a given height, $E_a(z)$, that is valid over either interface under horizontally homogeneous conditions

$$E_a(z) = \rho_a \overline{uw} U(z) + \rho_a \overline{we} + \overline{wp} \qquad \textbf{(12)}$$

where e and p are the kinetic energy and pressure fluctuations, respectively. The first term on the right-hand-side represents the flux of mean flow KE, while the last two terms represent the rate of diffusion of KE. Over land, we often assume that the energy flux through the ground is negligible, such that the flux entering the layer at height h can be related to the total rate of dissipation within the layer by

$$\rho_a \int_0^h \varepsilon \, dz = -E_a(h) + \frac{\rho_a g}{\Theta_v} \int_0^h \overline{w\theta_v} \, dz \qquad \textbf{(13)}$$

where ε is the dissipation of KE and Θ_v and θ_v denote the mean and fluctuating components of the virtual potential temperature. The second term on the right-hand-side accounts for the generation of KE due to any buoyancy flux. For neutral conditions, this expression states that the flux of KE into a layer is balanced by the total rate of dissipation within that layer. In horizontally homogeneous and stationary turbulence, the generation or transport of KE at a given height results from a non-zero vertical gradient of **(12)**. If the momentum flux is constant (i.e., a constant stress layer), then the vertical derivative of **(12)** gives the more familiar TKE budget equation

$$\varepsilon = -\overline{uw}\frac{\partial U}{\partial z} - \overline{vw}\frac{\partial V}{\partial z} + \frac{\partial \overline{we}}{\partial z} + \frac{1}{\rho_a}\frac{\partial \overline{wp}}{\partial z} + \frac{g}{\Theta_v}\overline{w\theta_v} \qquad \textbf{(14)}$$

where the terms of the right-hand-side of the TKE budget represent shear production, energy transport, pressure transport, and buoyant production, respectively. It is worth noting that a non-zero momentum flux divergence adds or subtracts from the mean kinetic energy of the flow (Tennekes and Lumley, 1972).

The KE budget given by **(14)** is one of the most commonly applied equations in investigation of the planetary boundary layers. When the fluctuations about the mean values are only driven by turbulence generated by shear instability or buoyant production, **(14)** is known as the turbulent kinetic energy (TKE) budget. Under these conditions, MO scaling provides a dimensionless form of the TKE budget given by

$$\frac{\varepsilon \kappa z}{u_*^3} = \phi_\varepsilon\left(\frac{z}{L}\right) = \phi_\varepsilon\left(\frac{z}{L}\right) - \phi_e\left(\frac{z}{L}\right) - \phi_p\left(\frac{z}{L}\right) - \frac{z}{L} \qquad \textbf{(15)}$$

where L is again the MO length. In a neutrally buoyant, constant flux layer over land where $\phi_\varepsilon(z/L=0) \approx 1$, the dissipation can be approximated by the well known wall-layer relationship

$$\varepsilon_p = \frac{u_*^3}{\kappa z} \qquad \textbf{(16)}$$

where ε_p is the predicted dissipation rate.

Over the ocean, the surface energy flux, which drives waves and currents, is no longer negligible, and **(13)** must be modified to take into account the total energy flux to the ocean surface. We can include this flux and rewrite **(13)** so that the surface energy flux appears on the left-hand-side as

$$E_a(0) = E_{aw} + E_{ao} = \rho_a \int_0^h \varepsilon\, dz + E_a(h) - \frac{\rho_a g}{\Theta_v}\int_0^h \overline{w\theta_v}\, dz \qquad \textbf{(17)}$$

where E_{aw} and E_{ao} represents the energy flux going directly into the waves and currents, respectively, where we are using the notation provided by Lionello et al. (1996). In the absence of stratification or buoyancy, **(13)** implies that the flux of KE in the marine surface layer is either 1) converted to thermal energy through viscous dissipation, 2) directly transferred to the current field, 3) or directly transferred to the wave field. The work required to overcome any stratification will consume some of the KE, while buoyancy will generate additional KE. The effect of thermal stratification thereby affects the amount of energy reaching the surface at a given wind speed.

This expression implies that less volume-averaged dissipation is required to balance the same energy flux over the ocean versus over land as long as there is a net flux into the ocean. Therefore, we would expect the flux of energy into the ocean to cause measured dissipation rates to differ from the wall layer prediction

given by **(16)** in the WBL, even if we include a means to account for stability. The presence of surface waves drives induced flow as we approach the surface, such that MO-similarity is expected to break down.

Investigations from the MBL/RASEX and CBLAST programs indicate that the departure from MO similarity is primarily due to two terms in the KE budget, i.e., the shear production and pressure transport terms. For example, any modification of the near surface wind profile due to wave forcing cannot be expected to obey MO scaling. Additionally, the energy transport between the atmospheric and ocean waves is given by

$$E_{aw} \approx \int c(\omega)\tau(\omega)\,d\omega \approx \overline{p_\eta \frac{\partial \eta}{\partial t}} \qquad \textbf{(18)}$$

where ω is the wave frequency; and are the phase speed and surface stress supported by waves of that frequency, is the pressure at the surface, is the instantaneous wave height and is the wave slope. This term couples the KE energy budget to the ocean surface since it represents the boundary conditions for the pressure transport term in **(14)**. Therefore, the behavior of this flux (i.e., its gradient) is expected to impact the KE budget in the WBL. Either of these effects is expected to lead to a breakdown of similarity relationships like **(15)** within the WBL.

5.1. Dissipation Deficit and Wave Growth

The hypothesis that the dissipation profiles are influenced by wave-induced flow near the ocean surface implies that MO-similarity must break down in the wave boundary layer. We can investigate this hypothesis by comparing the vertical profiles of the dissipation rate with their MO-similarity prediction:

$$\varepsilon_p = \frac{u_*^3}{\kappa z}\phi_\varepsilon(z/L) \qquad \textbf{(19)}$$

using the form of the dimensionless dissipation function given by Edson and Fairall (1998)

$$\phi_\varepsilon(\xi) = \frac{(1-\xi)}{(1-7\xi)} - \xi \qquad \xi < 0 \qquad \textbf{(20)}$$

$$\phi_\varepsilon(\xi) = 1 + 5\xi \qquad \xi > 0 \qquad \textbf{(21)}$$

For example, under conditions of developing waves we would expect an energy flux into the ocean and less dissipation than the wall-layer prediction given by MO similarity:

$$\varepsilon < \varepsilon_p = \frac{u_*^3}{\kappa z}\phi_\varepsilon(z/L) \qquad \textbf{(22)}$$

This dissipation deficit, i.e., the imbalance between production and dissipation, has been predicted by Janssen (1999). Evidence for this is shown in Figure 10, which shows that the measured dissipation profiles are less than their MO-similarity prediction, which can be thought of as a dissipation deficit. These measurements are averaged over a 2-hour period of increasing winds and growing seas.

The time series of the various energy flux terms from **(12)** taken during the MBL program on the R/P FLIP are shown in Figure 11. The dissipation profile is found by fitting a line to ε versus $1/z$ and then integrating from .001 m to 14 m. The figure shows that the dominate terms in this expression is the volume averaged dissipation rate and the mean flow KE. The diffusion terms are much smaller at this height and tend to be of different sign. The effect of stratification on the energy flux is negligible except at the lowest wind speeds. At all other wind speeds the volume averaged-dissipation is less than the mean flow KE, and the

difference is not balanced by the remaining terms. The net result is that production exceeds dissipation and the surface energy flux is nonzero.

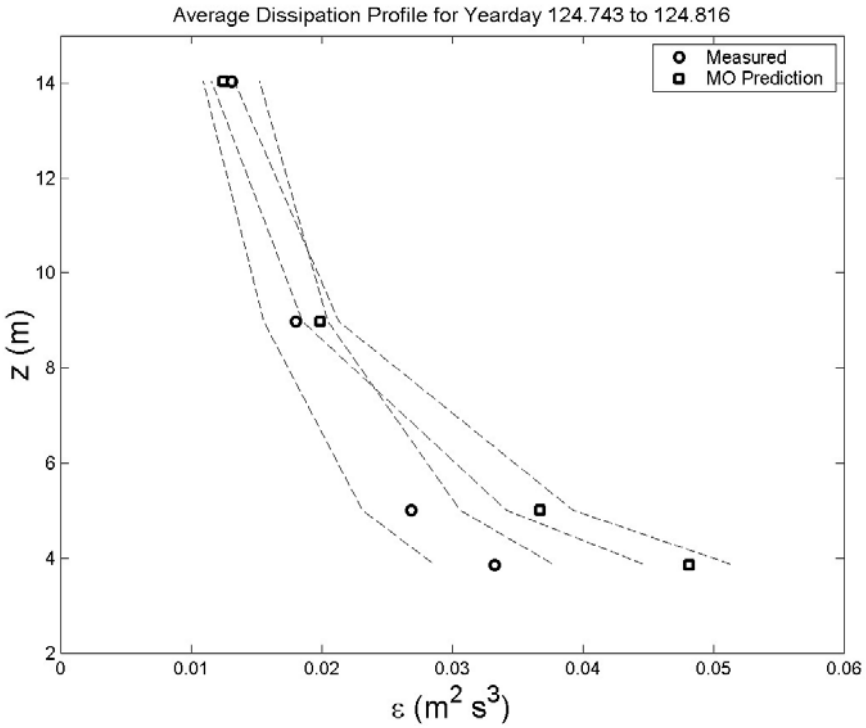

Figure 10. Profiles of measured and predicted dissipation rates using (24) during a 2 hour period. The symbols represent the mean values and the dashed lines represent plus or minus the standard deviation about theses means.

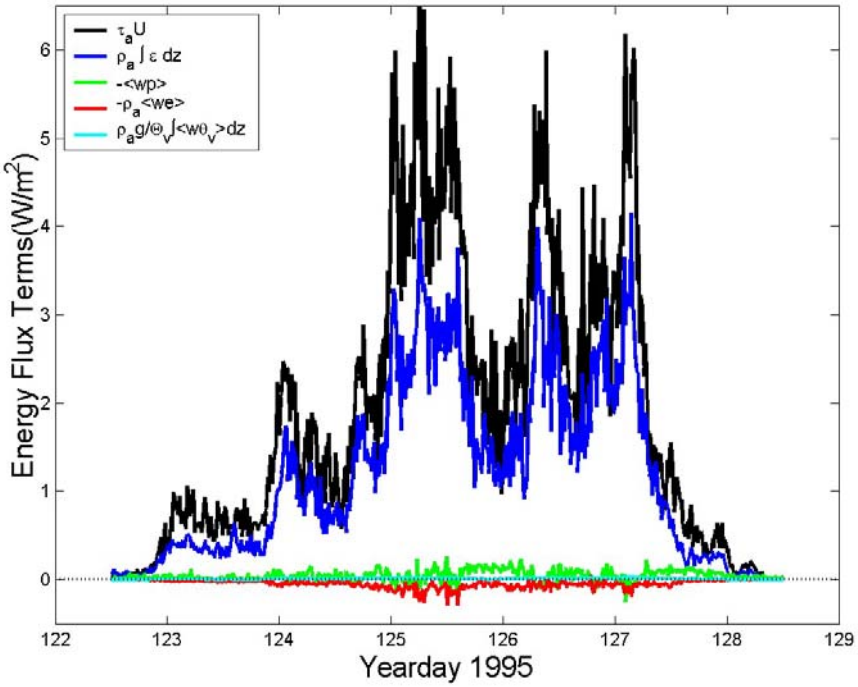

Figure 11. Time series of the terms in the energy flux given by (12) plotted with the layer integrated dissipation and heat flux as given in (17) from t he R/P FLIP.

These terms are combined using **(17)** to produce estimates of the surface energy flux, $E_a(0)$. This estimate can be compare with the approach used by most wave modelers that relates the energy flux to the wave spectrum using a wave growth parameter

$$E_{aw} = -\rho_w g \iint \Gamma S_\eta(\omega,\theta) d\omega d\theta \qquad \textbf{(23)}$$

where ρ_w is the density of sea water, S_η is the directional wave spectrum, and Γ is the growth-rate parameter. The two estimates are compared in Figure 12, where commonly used estimates of Γ are given by Donelan and Pierson (1987) and Plant (1982) formulations and the wave spectra are computed using wave-wire measurements from FLIP. The energy fluxes computed by previous parameterizations closely follows our estimates of E_{aw}. The good agreement suggests that the imbalance between production and volume averaged dissipation results in an accurate estimate of the energy flux to the ocean surface.

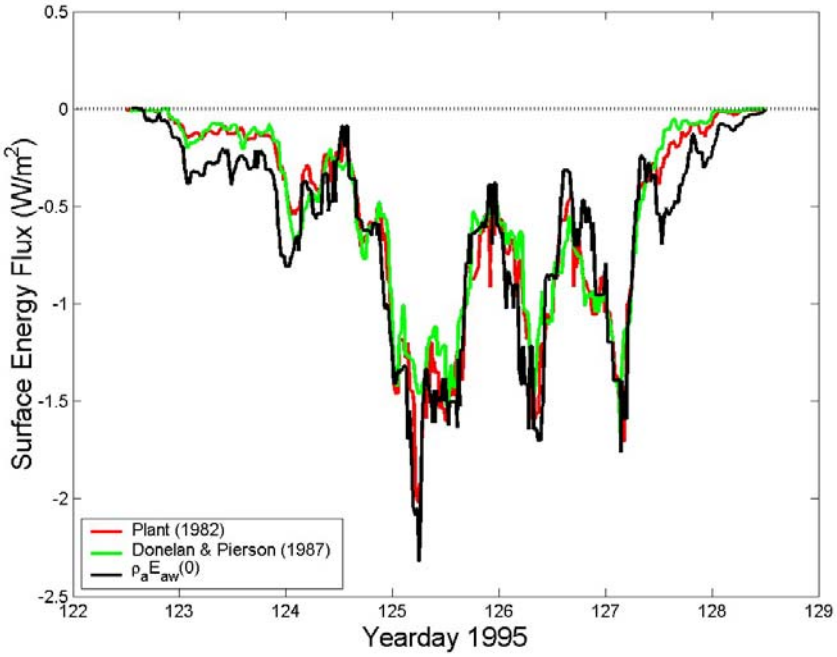

Figure 12. Estimates of the surface energy flux from the atmosphere to surface waves using (17). The other estimates are found from (23) using our measured wave spectra with the growth rate parameterization of Plant (1982) and Donelan and Pierson (1987).

5.2. Dissipation Surplus and Swell

Although it is difficult to see on the displayed axes, there are instances under low wind conditions where the volume averaged dissipation exceeds the mean flow KE entering at 14 m. These conditions correspond to decaying seas where the phase speed of the swell is greater than the overlying wind speed. As a result, the upward energy flux from the component of the wave spectrum where the waves are moving faster than the wind can results in an upward total energy flux. Swell dominated conditions were commonly found during the CBLAST program and estimates of the energy flux from **(17)** show clearer instances where the flux is out of the ocean. For example, in Figure 13 there are periods around Yearday 195 and 199 where the integrated dissipation is greater than the mean flow KE. However, it is also worth noting that the scale of the y-axis is approximately 6 times smaller than the scale shown in Figure 11. Therefore, the transfer of energy

is substantially smaller under the light wind conditions experienced during much of the CBLAST experiment.

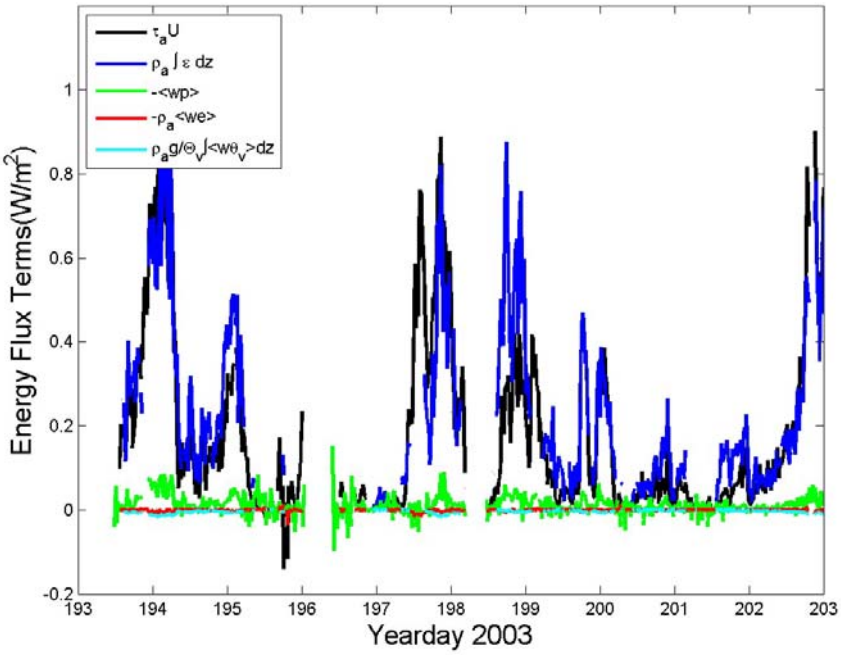

Figure 13. Time series of the terms in the energy flux given by (12) plotted with the layer integrated dissipation and heat flux as given in (17) from t he ASIT during CBLAST.

5.3. Implications

The observed departure from traditional wall-layer scaling can have a significant impact on methods used to estimate the flux. For example, the inertia-dissipation method is commonly used to estimate the momentum flux at sea. In this method, velocity spectra are used to provide inertial subrange estimates of the dissipation rate, which are fairly insensitive to the lower frequency motion of the ship. The momentum flux is then estimated using the dissipation rate and the parameterization of ϕ_ε:

$$\tau = \rho_a u_*^2 = \rho_a \left(\frac{\varepsilon \kappa z}{\phi_\varepsilon (z/L)} \right)^{2/3} \qquad \textbf{(24)}$$

This type of parameterization should be valid as long as the measurements are made above the WBL and the constant flux assumption holds. These conditions are reasonably well met at the measurements heights used on most research vessels (e.g., Edson and Fairall, 1998). However, the results shown in Figure 10 indicate that these may not be a reasonable assumption on measurement heights associated with surface moorings (i.e., buoys).

Finally, it is hypothesized that an upward total energy flux is more common than an upward total momentum flux because of the multiplication of the large phase speed associated with swell given in **(18)**. In generally, longer waves are likely to have a greater impact on energy transfer than momentum transfer under all conditions. As such, the WBL for energy is expected to extend higher into the marine surface layer than the WBL for momentum. This may also explain why flux estimates from the bulk method now appear to be more accurate than the inertial-dissipation method.

6. Summary

Recent field experiments have confirmed that MO similarity is generally valid in the marine surface layer. The main exception is under low wind, swell conditions where MO similarity is not applicable due to wave driven flow very near the surface. These wave-driven processes have a strong impact on the pressure transport term in the KE budget. However, flux-profile relationships based on the dimensionless shear and scalar gradient functions remain are in good agreement with measurements over a wide range of conditions. As with land-based results, there is greater uncertainty in these functions under stratified conditions. It should be noted that stratified conditions are commonly encountered in the marine surface layer; particularly in the spring and early summer over regions with strong wintertime cooling and over regions of strong coastal upwelling.

Recommendation: We recommend the continued use of functions based on MO-similarity theory in numerical models of the marine surface layer.

The drag coefficient is constant over a rigid surface, but varies over the ocean due to surface waves. Therefore, the drag coefficient has often modeled as a function of the "age" of the waves, where developing or "young" waves tend to enhance the drag while decaying or "old" waves (i.e., swell) tend to reduce the drag at any given wind speed. It is only natural to take advantage of ECMWF's coupled atmosphere-wave models and use a sea-state dependent drag coefficient. The implementation of this parameterization in a coupled model will also require some tuning. The same can be said for the transfer coefficients of heat and momentum. However, the transfer coefficients used in the model should match the wind speed dependent transfer coefficients within the uncertainty of the measurements. This includes the observed linear increase of the transfer coefficients for heat and mass with wind speed, which is also predicted by semi-empirical theory. A good candidate model for model comparison is the widely used COARE 3.0 algorithm. This algorithm is based on directly measured fluxes and means collected during a number of field programs starting with the TOGA-COARE experiments in the early 90's. CLIMODE measurements filled an important data gap at high wind speeds. Addition of this new data lead to minor changes to the coefficients in the COARE 4.0 algorithm which translates to higher fluxes at wind speeds over 15 m/s.

A very interesting outcome of this workshop is the similarity between initial comparisons of the COARE 4.0 algorithm with the results found from ECMWF's coupled model. Specifically, the COARE algorithm matches the observations well without any wave information. Furthermore, it is nearly identical to the function representing the globally averaged drag coefficient from a wave-age based model run at ECMWF. This begs the question: **Why do wave-age and wind-speed dependent formulation give such similar results?** The answer is found in the wind and wave data; namely, in storm passage after storm passage, the wave-age varies nearly linearly with wind-speed. The composite of all these storms shows that young waves are almost always found under high wind conditions, and old waves are found in their wake after winds have calmed down. Therefore there is not a pronounced functional difference between drag coefficients based on wind-speed and on wave-age – at least over the open ocean up to approximately 25 m/s. However, this good comparison holds in the mean and it is not clear whether the wind-speed or wave-age dependent formulation is more accurate. Shallow water and fetch-limited conditions still pose problems to both approaches, and considerable uncertainty remains about the behavior of the drag coefficient at the extreme wind conditions found under tropical cyclones and hurricanes.

At very low winds, observations have shown that non-locally generated waves (swell) can have a significant impact on momentum transfer. They provide momentum to the atmosphere when the

wind and swell are aligned, which acts to reduce the drag and the total (wind plus wave) momentum flux. Observations have also shown that they enhance the drag when the swell propagates against the wind (counter swell). However, the momentum flux remains small under these low wind conditions and it is not clear whether this will have a significant impact on forecasts.

Lastly, there is substantially less community consensus on the behavior of the transfer coefficients at stronger winds. As such, we cannot make any strong recommendations for use of transfer coefficients under these conditions. Instead, the form of the transfer coefficients that give reasonable predictions of, particularly, wind speed and wave heights provide significant insight on the nature of heat, mass and momentum transfer under extreme winds.

Recommendation: The surface flux parameterizations used at ECMWF should agree the COARE algorithm within 10% for momentum (drag) and 30% for heat and mass up to approximately 20 m/s. It appears from our initial comparisons that this has already been accomplished for the drag coefficient at moderate to high wind conditions. At low wind speeds, it is not clear whether the wave-driven wind situation will have an impact on weather forecasts due to the small magnitude of the stress under these conditions. However, ECMWF's use of a wave model to provide the surface stress can mimic these conditions. Therefore, we recommend that the stress parameterization be adjusted to allow upward momentum flux under these conditions. Lastly, we cannot recommend any particular formulation at extreme wind speeds other than the requirement that they agree with COARE at lower winds. However, the form of the parameterizations that give reasonable agreement between the model and available observations provide useful information to the marine science community.

Additionally, observations have shown that the stress and wind vectors become unaligned when the wind and waves are unaligned but the atmosphere and ocean remain strongly coupled. Observations have shown that the direction of the stress vector lies somewhere between the wind and wave directions. Such conditions are commonly encountered during frontal passages with moderate to strong winds. Presumably, similar situations are found in hurricanes where the wind and waves are often unaligned for a variety of reasons. However, it is unclear whether this misalignment has a significant impact on model forecasts, particularly if the magnitude of the stress is properly modeled.

Recommendation: It would be a useful exercise for the observational community to test how sensitive the model forecast is to this misalignment. For example, the two runs could be conducted where the stress is aligned with the wind in one case and the dominant waves in the other. A significant difference in the model output would provide motivation for further study for both the observations and modeling communities.

7. References

Charnock, H., 1955: Wind stress on a water surface, *Quart. J. Roy. Soc.*, **81**, 639-640.

Donelan, M. A., F. W. Dobson, S. D. Smith and R. J. Anderson, 1993: On the dependence of sea surface roughness on wave development, *J. Phys. Oceanogr.*, **23**, 2143-2149.

Edson, J., T. Crawford, J. Crescenti, T. Farrar, N. Frew, G. Gerbi, C. Helmis, T. Hristov, D. Khelif, A. Jessup, H. Jonsson, M. Li, L. Mahrt, W. McGillis, A. Plueddemann, L. Shen, E. Skyllingstad, T. Stanton, P. Sullivan, J. Sun, J. Trowbridge, D. Vickers, S. Wang, Q. Wang, R. Weller, J. Wilkin, A. Williams, D.K.P. Yue, and C. Zappa, 2007. The Coupled Boundary Layer and Air-Sea Transfer Experiment in Low-winds (CBLAST-LOW). *Bulletin of the American Meteorological Society,* **88**, 341-356

Edson, J. B., R. F. Crofoot, W. R. McGillis, and C. Zappa, 2006: Investigations of flux-profile relationships in the marine atmospheric surface layer during CBLAST, 16th Symp. on Boundary Layers and Turbulence, Portland, ME Ref. 8.2, AMS, Boston, MA.

Edson, J. B., and C.W. Fairall, 1998: Similarity relationships in the marine atmospheric surface layer for terms in the TKE and scalar variance budgets, *J. Atmos. Sci.,* **55**, 2311-2328.

Fairall, C. W., E. F. Bradley, J. E. Hare, A. A. Grachev, and J. B. Edson, 2003: Bulk parameterization of air–sea fluxes: Updates and verification for the COARE algorithm, *J. Climate*, **16**, 571–591.

Hare, J.E., T. Hara, J.B. Edson, and J.M. Wilczak, 1997: A similarity analysis of the structure of air flow over surface waves, *J. Phys. Oceanogr.,* **27**, 1018-1037.

Hristov, T. S., S. D. Miller, and C. A. Friehe, 2003: Dynamical coupling of wind and ocean waves through wave-induced air flow, *Nature,* **422**, 55-58.

Janssen, P. A. E. M., 1999: On the Effect of Ocean Waves on the Kinetic Energy Balance and Consequences for the Inertial Dissipation Technique. *J. Phys. Oceanogr.,* **29**, 530 - 534.

Johnson, et al., 1998: On the dependence of sea surface roughness on wind waves, *J. Phys. Oceanogr*., **28**, 1702-1716.

Lionello, P., K. Hasselmann, and G.L. Mellor, 1996: On the coupling between a surface wave model and a model of the mixed layer in the ocean. *The Air-Sea Interface: Radio and Acoustic Sensing, Turbulence and Wave Dynamics*, M.A. Donelan, W. H. Hui and W.J. Plant, Eds, University of Toronto Press, 195-201.

Mahrt, L., D. Vickers, J. Howell, J. Højstrup, J.M. Wilczak, J.B. Edson, and J.E. Hare, 1996: Sea surface drag coefficients in RASEX, *J. Geophys. Res.,* **101**, 14327-14335.

Miles, J. W., 1957: On the generation of surface waves by shear flows. *J. Fluid Mech.,* **3**, 185-204.

Monin, A.S., and Obukhov, A.M., 1954: Basic laws of turbulent mixing in the surface layer of the atmosphere. *Tr. Akad. Nauk SSSR, Geofiz Inst.,* **151**, 163-87.

Obukhov, A.M., 1946: Turbulence in an atmosphere with a non-uniform temperature. *Tr. Akad. Nauk.USSR, Inst. Teoret. Geofiz,* **1**. Translated and published in *Bound.-Layer Meteor.,* **2**, 7-29, 1971.

Plant, W. J., 1982: A relationship between wind stress and wave slope. *J. Geophys. Res*, **87**, 1961-1967.

Sullivan, P. P., J. B. Edson, T. Hristov, and J. C. McWilliams, 2008: Large eddy simulations and observations of atmospheric marine boundary layers above non-equilibrium surface waves, *J. Atmos. Sci.,* **65**, 1225-1245.

Vickers, D. and L. Mahrt, 1999: Observations of non-dimensional wind shear in the coastal zone, *Quart. J. Roy. Met. Soc.*, **125**, 2685-2702.